14. Letourner, F. *et al.* Coatomer is essential for retrieval of dilysine-tagged proteins to the endoplasmic reticulum. *Cell* **79,** 1199–1207 (1994).
15. Harter, C. & Wieland, F. T. A single binding site for dilysine retrieval motifs and p23 within the gamma subunit of coatomer. *Proc. Natl Acad. Sci. USA* **95,** 11649–11654 (1998).
16. Bremser, M. *et al.* Coupling of coat assembly and vesicle budding to packaging of putative cargo receptors. *Cell* **96,** 495–506 (1999).
17. Erickson, J. W., Cerione, R. A. & Hart, M. J. Identification of an actin cytoskeletal complex that includes IQGAP and the Cdc42 GTPase. *J. Biol. Chem.* **272,** 24443–24447 (1997).
18. Kreis, T. Microinjected antibodies against the cytoplasmic domain of vesicular stomatitis virus glycoprotein block its transport to the cell surface. *EMBO J.* **5,** 931–941 (1986).
19. Musch, A., Xu, H., Shields, D. & Rodriguez-Boulan, E. Transport of vesicular stomatitis virus G protein to the cell surface is signal mediated in polarized and nonpolarized cells. *J. Cell Biol.* **133,** 543–558 (1996).
20. Dascher, C. & Balch, W. E. Dominant inhibitory mutants of ARF1 block endoplasmic reticulum to Golgi transport and trigger disassembly of the Golgi apparatus. *J. Biol. Chem.* **269,** 1437–1448 (1994).
21. Wu, W., Lin, R., Cerione, R. A. & Manor, D. Transformation activity of Cdc42 requires a region unique to Rho-related proteins. *J. Biol. Chem.* **273,** 16655–16658 (1998).
22. Kroschewski, R., Hall, A. & Mellman, I. Cdc42 controls secretory and endocytic transport to the basolateral plasma membrane of MDCK cells. *Nature Cell Biol.* **1,** 8–13 (1999).
23. Erickson, J. W., Zhang, C. J., Kahn, R. A., Evans, T. & Cerione, R. A. Mammalian Cdc42 is a brefeldin A-sensitive component of the Golgi apparatus. *J. Biol. Chem.* **271,** 26850–26854 (1996).
24. Lin, R., Cerione, R. A. & Manor, D. Specific contributions of the small GTPases Rho, Rac, and Cdc42 to Dbl transformation. *J. Biol. Chem.* **274,** 23633–23641 (1999).
25. Bershadsky, A. D. & Futerman, A. H. Disruption of the Golgi apparatus by brefeldin A blocks cell polarization and inhibits directed cell migration. *Proc. Natl Acad. Sci. USA* **91,** 5686–5689 (1994).
26. Peranen, J., Auvinen, P., Virta, H., Wepf, R. & Simons, K. Rab8 promotes polarized membrane transport through reorganization of actin and microtubules in fibroblasts. *J. Cell Biol.* **135,** 153–167 (1996).
27. White, M. A. *et al.* Multiple Ras functions can contribute to mammalian cell transformation. *Cell* **80,** 533–541 (1995).
28. Westwick, J. K. *et al.* Rac regulation of transformation, gene expression, and actin organization by multiple, PAK-independent pathways. *Mol. Cell. Biol.* **17,** 1324–1335 (1997).
29. McCallum, S. J., Erickson, J. W. & Cerione, R. A. Characterization of the association of the actin-binding protein, IQGAP, and activated Cdc42 with Golgi membranes. *J. Biol. Chem.* **273,** 22537–22544 (1998).
30. Bagrodia, S., Taylor, S. J., Jordan, K. A., Van Aelst, L. & Cerione, R. A. A novel regulator of p21-activated kinases. *J. Biol. Chem.* **273,** 23633–23636 (1998).

Acknowledgements

We thank C. Harter and F. Wieland for the anti-α/γCOP antibody and the cDNA for γCOP; A. Musch for advice on VSV-G transport assays; J. Lippinoctt-Schwartz for the plasmid expressing VSV-G; and C. Westmiller for secretarial assistance. We also acknowledge support from the National Institutes of Health.

Correspondence and requests for materials should be addressed to R.A.C. (e-mail: rac1@cornell.edu).

Two-headed binding of a processive myosin to F-actin

Matthew L. Walker*, Stan A. Burgess*, James R. Sellers†, Fei Wang†, John A. Hammer III‡, John Trinick* & Peter J. Knight*

* *Astbury Centre for Structural Molecular Biology, School of Biomedical Sciences, University of Leeds, Leeds LS2 9JT, UK*
† *Laboratories of Molecular Cardiology and* ‡ *Cell Biology, National Heart, Lung and Blood Institute, National Institutes of Health, Bethesda, Maryland 20892, USA*

Myosins are motor proteins in cells. They move along actin by changing shape after making stereospecific interactions with the actin subunits[1]. As these are arranged helically, a succession of steps will follow a helical path. However, if the myosin heads are long enough to span the actin helical repeat (~36 nm), linear motion is possible. Muscle myosin (myosin II) heads are about 16 nm long[2], which is insufficient to span the repeat[3]. Myosin V, however, has heads of about 31 nm that could span 36 nm (refs 4, 5) and thus allow single two-headed molecules to transport cargo by walking straight[5]. Here we use electron microscopy to show that while working, myosin V spans the helical repeat. The heads are mostly 13 actin subunits apart, with values of 11 or 15 also found. Typically the structure is polar and one head is curved, the other straighter. Single particle processing reveals the polarity of the underlying actin filament, showing that the curved head is the leading one. The shape of the leading head may correspond to the beginning of the working stroke of the motor. We also observe molecules attached by one head in this conformation.

Myosin V is a class of motor protein implicated in vesicle transport in cells and is particularly abundant in neurons[1]. The kinetics of its ATPase show differences from those of myosin II (muscle myosin) which may be adaptations for hand-over-hand 'processive' action[6,7]. Thus the rate of ADP release from the complex with actin is close to the overall cycle rate, whereas ATP binding and cleavage are much faster. The affinity of myosin V–ADP for actin is very high. These properties ensure that the heads are attached to actin for a larger fraction of the ATPase cycle than myosin II, that is, their duty ratio is higher. For fully processive motion by this mechanism, one head should not detach before the second re-attaches. Although this is the case for two-headed motors that move along microtubules[8,9], it is controversial whether myosin V typically takes many or few steps before detaching[10,11].

The structural basis of the processive movement has not been established. Early electron microscopy of the complex of myosin V and actin found bundles of filaments crosslinked by the two heads[4], in the manner previously seen with myosin II (ref. 12). When excess myosin V was present, fully decorated actin was found with a fringe of material about 50 nm wide. Some of this was fine strands, probably the tails, but some appeared more globular, suggestive of molecules attaching by a single head. Binding of both heads to a single actin filament was not reported. The two heads of myosin II can attach to the same filament, and are generally on adjacent subunits, only occasionally on the next but one[3]. To understand processive movement, it is therefore important to show whether, and under what conditions, the two heads of myosin V can bind to a single actin filament.

Optical trap records show that at 1 μM ATP, steps occur at about one-second intervals[10]. This rate is limited by the rate of ATP binding, and we reasoned that this should favour observation of molecules attached by both heads: the trailing one being free of nucleotide, the lead one probably at an earlier stage in the cycle. To see the structure of individual molecules attached to actin we mixed a low molar ratio of myosin V HMM (heavy meromyosin, that is, lacking the cargo-binding domain) with actin under these conditions. This myosin has a high affinity for actin, so we were able to avoid ATP depletion by using only 40 nM HMM; we also used ~100 mM ionic strength, in contrast to the requirements for observing myosin II during ATPase activity[13]. We observed about 50% of the bound molecules attached by both heads (Fig. 1a–d). The heads are spaced far apart along actin, as required for linear processive function, and attachment to adjacent actin subunits was not observed. There were also many singly attached (Fig. 1e) and unattached molecules, and many of the actin filaments were bundled together. Myosin V purified from chick brain[14] and myosin V HMM stored in excess calmodulin gave very similar results (data not shown), indicating that the wide separation of the attached heads is not an artefact of a misfolded or calmodulin-depleted preparation. Doubly-attached heads became rare if the grid was rinsed with a higher concentration of ATP, as expected if the trailing head is free of nucleotide.

In the absence of ATP or ADP, we found a strong tendency towards bundling of actin filaments by myosin V HMM, and the structure within these bundles was obscure. By using more dilute proteins and allowing only a few seconds between mixing and adsorption to the carbon film, we reduced bundling. We observed very few unattached molecules under these conditions, indicating that almost all the myosin was competent in actin binding. Many myosin molecules were attached by only one head, but the doubly-attached molecules appeared similar to those in Fig. 1a–d. The

presence of molecules with only one head attached, and the strong bundling tendency, indicate that it is relatively difficult for two nucleotide-free myosin V heads to bind to the same actin filament. In rigor the two heads have the same preferred conformation and there would have to be substantial distortion in the second head to allow binding to the same filament.

In the presence of saturating ATP (1.0 mM), we observed many more unattached molecules, indicating that myosin V HMM is not strongly processive. Those that were attached bound almost exclusively by one head, and bundling was infrequent.

ADP slows the rate of actomyosin V ATPase by forming an actin–myosin–ADP intermediate. As this is a tight binding complex for myosin V (ref. 6), ADP should favour two-headed binding. In the absence of ATP, 20 μM ADP reduced bundling compared to rigor, and more doubly-attached molecules were present. This indicates that the actin binding properties of myosin V HMM–ADP are different from those of nucleotide-free heads. Addition of 2 μM ADP to 1 μM ATP caused an increase in bundling, but had little effect on the incidence of double attachment. Addition of 100 μM ADP to 100 μM ATP increased the fraction of molecules attached, the amount of bundling and the incidence of doubly-attached molecules. Thus the incidence of double attachment follows the expectations from the kinetic properties of myosin V (refs 6, 7).

To determine the separation between the heads of doubly-attached molecules we applied single particle image processing[15–17], using the actin subunit periodicity to calibrate the magnification of the micrographs. Figure 2 shows that the heads were typically 13 actin subunits apart, a distance of 36 nm. With 13/6 actin helical symmetry, these strides will produce linear motion. Figure 2 also shows subsidiary peaks of 11 and 15 subunits between attached heads (30 nm and 41 nm, respectively). These subunits are azimuthally adjacent to subunit 13. Molecules with different stride lengths appeared similar in other respects (Fig. 1b–d). This variation may be a consequence of cumulative angular disorder in actin filaments[18], sometimes bringing subunits 11 or 15, rather than subunit 13, to the same azimuth as the first. Flexibility within the myosin may also contribute, allowing heads to vary the azimuth as well as the distance at which they attach. Variation in stride length may thus contribute to the variation in step size measured in optical trap experiments.

Most doubly-attached molecules (70%) show an obvious polarity because both heads are curved in the same direction, though to different degrees, like a skier's legs in the telemark stance (Fig. 1a–d). Where more than one telemark-shaped molecule was attached to a single actin filament they all showed the same polarity (Fig. 1a), indicating that this structure is not merely a random distortion. To determine the polarity of the telemark shape relative to that of F-actin, we aligned short (48 nm) segments of F-actin to which heads were attached to generate a polar average (Fig. 1f). Inspection of the HMM molecules attached to the aligned segments showed that for the great majority (82% of 203 molecules) the barbed end of the filament was beyond the strongly curved head. As the direction of movement of this

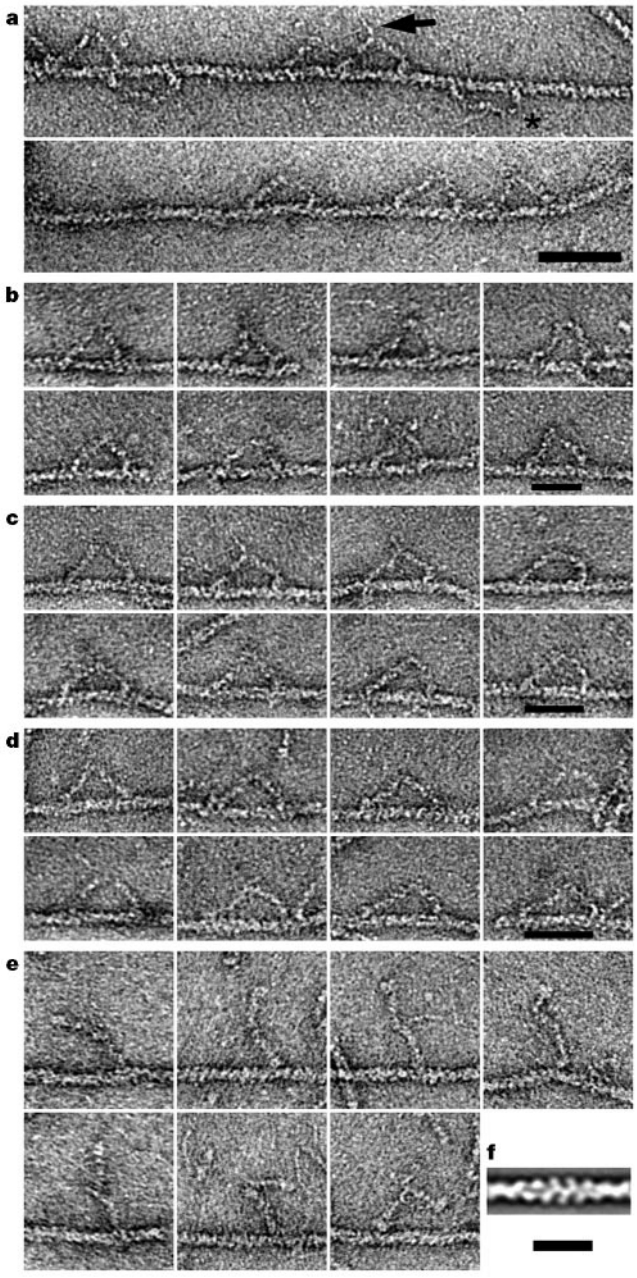

◀ **Figure 1** Structure of myosin V HMM bound to F-actin. All filaments are shown with the barbed end to the right. **a**, Filaments with several examples of two-headed binding in 1 μM ATP. Arrow, an HMM tail pointing away from the barbed end of the actin; asterisk, W-shaped molecule. **b**–**d**, Galleries of single HMM molecules spanning 11, 13 and 15 actin subunits respectively; left column shows symmetrical structure, the others the polar telemark structure, orientated with the leading head to the right; bars correspond to a distance of 11 (**b**), 13 (**c**) or 15 (**d**) subunits. **e**, Examples of single-headed binding in 1 μM ATP, arranged to simulate a plausible walking cycle (see Fig. 4; also animated at http://www.leeds.ac.uk/bms/research/muscle/muscle.htm). **f**, Typical average of aligned segments of F-actin underlying myosin V heads. Scale bar in **a** 50 nm; applies to **a**–**e**, **f,** 20 nm. We expressed the HMM-like fragment of mouse myosin Va heavy chain[7] (residues 1–1,091) and calmodulin by co-infection of Sf9 cells by baculovirus vectors, purified them as described[7] and stored them at ~1.6 μM in 0.5 M KCl, 0.1 mM EGTA, 1 mM dithiothreitol, 10 mM MOPS, pH 7.0. Actin was from rabbit skeletal muscle, stored in liquid N_2 at 220 μM in 0.2 mM $CaCl_2$, 0.5 mM DTT, 0.2 mM ATP, 2 mM Tris–HCl, pH 8.0 at 0 °C. We formed the Mg polymer by addition of 0.2 mM EGTA and 0.1 mM $MgCl_2$, followed after 15 min by 50 mM KCl. We diluted the proteins using 0.10 M KCl, 1.0 mM EGTA, 1.0 mM $MgCl_2$, 10 mM MOPS, pH 7.0. We made specimens from equal volumes of F-actin (0.4–1.6 μM) and myosin V HMM (0.08–0.16 μM), mixed and immediately applied to carbon-filmed EM grids as described[25]. We stained the grids with 1% uranyl acetate, generally without rinsing as this washed away cycling molecules. For rigor and ADP experiments, we treated 40 μM F-actin with 0.01 units ml^{-1} apyrase (Sigma A6535) for 5 min before use. When needed, we incubated 40 μM ADP for ~2 min with the HMM only before mixing with actin. When used, we added ATP to both proteins 5 s before they were mixed. We calibrated micrographs at ×40,000 using Fourier transforms of straight segments of F-actin, and scanned (Leafscan-45) at a step size corresponding to 0.53 nm at the specimen. Image processing was performed using the SPIDER software suite[26].

myosin along actin is towards the barbed end[4], this indicates that the strongly curved head leads and the straighter one trails. We suppose that the remainder, with reversed polarity, originate from incorrectly assigned actin polarity, as these were more numerous where the actin structure correlated weakly with the average. With the direction of movement determined, we can also observe that the short HMM tail is typically angled in the trailing direction (for example, Fig. 1a, arrow). About 30% of doubly-attached molecules show sufficiently little difference in shape between the heads that polarity is not apparent (Fig. 1b–d, left). Molecules with this structure were found in all experiments. Molecules are also seen that are W- rather than V-shaped (Fig. 1a, asterisk). We suspect that these are attached to actin at azimuths that place them out of the plane of the carbon film, and that their appearance is a consequence of collapse.

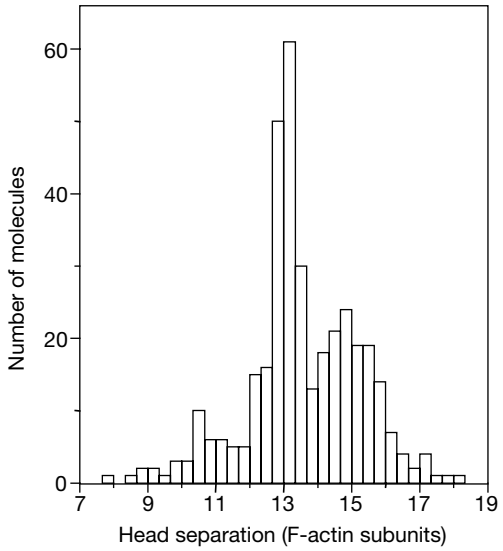

Figure 2 Axial distance spanned by two heads of a myosin V HMM molecule attached to actin in 1 μM ATP. The distance between heads was measured by aligning the motor domains and using the resulting rotation and translation parameters to determine their positions in the original micrographs. $n = 367$. Specimens prepared in 20 μM ADP also gave a peak separation of 13 subunits.

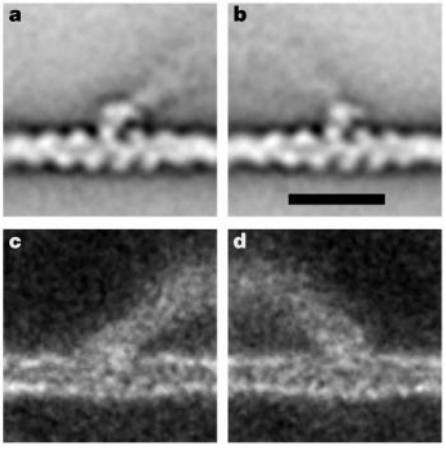

Figure 3 Average and variance images respectively of 262 lead (**b**, **d**) and 234 trail (**a, c**) heads of myosin V HMM bound to actin in the presence of 1 μM ATP. Scale bar: 20 nm. We aligned the underlying actin first, then aligned the lead and trail heads using a mask that essentially excluded the actin. The clarity of the actin structure indicates that these averages derive from heads bound to a narrow range of actin azimuths.

Image averaging (Fig. 3) shows that both motor domains are primarily associated with single actin subunits and are similar in shape. The actin subunits to which they attach appear the same. Variation in shape between molecules weakens the light chain domains in the averages, but the variance images (Fig. 3c, d) indicate the range of shapes. The trailing light chain domain emerges from the leading side of the motor domain and is angled at roughly 40° to the filament (Fig. 3a); this resembles the rigor angle[19], thought to be the end of the working stroke. The averaged structure of the leading head is quite different as its light chain domain emerges near the trailing side of the motor domain and is strongly angled back to join the other head. The angle to the filament, measured near the junction of the light chain domain with the motor domain, varies between individual images with a range of 90–150°; from the average image (Fig. 3b), the angle is about 115°. Comparing the averages there is thus a pronounced (75°) difference between the two heads in the orientation of the light chain domain emerging from the motor domain, and this is in the direction expected to produce a forward working stroke by the leading head once the trailing head detaches. Rotation through this angle would produce an axial translation of 26 nm for the head–tail junction of an unconstrained head. Laser trap measurements of single working strokes by myosin V give similar values (~20 nm)[11,20], which indicates that the images are relevant to the start and end of the working stroke.

The telemark-shaped molecules may show us two key states of the processive motion (Fig. 4). Evidence is accumulating for a strain dependence in ADP release in this and other myosins[6,19,21]. The structure we have observed for the leading head is that predicted to correspond to the direction of strain that would inhibit ADP release, whereas the trailing head is strained in the direction likely to promote release. Thus it is plausible that in images obtained at low ATP concentrations, the trailing head is nucleotide-free and the leading head may still contain ADP. Detachment of the trailing head by ATP allows the leading head to tilt forward, carrying the detached

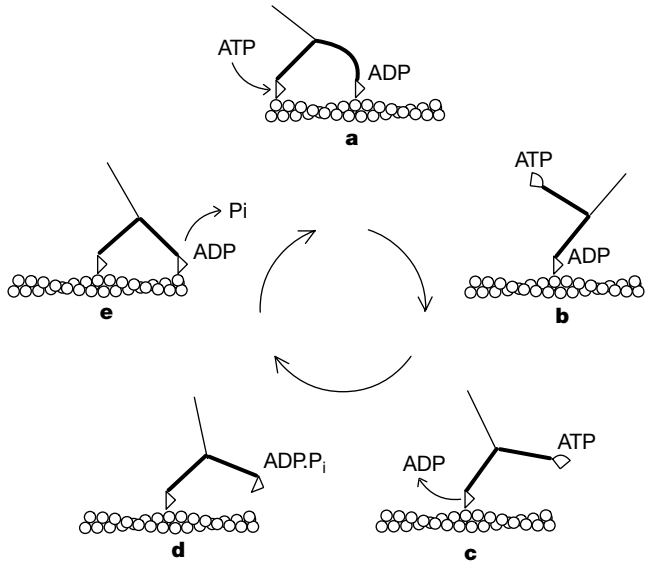

Figure 4 Model showing the role of two-headed attachment in the walking cycle of myosin V. The trailing, nucleotide-free head of a telemark-shaped molecule binds ATP (**a**) and detaches, relieving the axial strain in the molecule (**b**) and bringing the detached head towards the next actin site (**c**). Dissociation of ADP completes the working stroke (**d**). Attachment of the free head is quickly followed by loss of phosphate by actin activation, and a tight binding develops (**e**). The detached head is shown in two conformations to indicate the transitions to a weak binding, followed by a primed conformation indicated by crystal structures of myosin II heads[23,24].

head towards its next binding site. Rebinding could be facilitated by the sharp angle induced between motor and lever arm on ATP binding[22–24], as this would resemble the structure we see for the leading head. The shape of the leading head is the start of the walking stride, and the trailing head the end.

The relationship between the working stroke of a single myosin V head and the 36-nm walking stride of the two-headed molecule requires clarification. As mentioned, the working stroke has been estimated at ~20 nm in the laser trap[11,20] and ~26 nm here. These values fall well short of the ~36 nm span seen here, indicating that some additional flexibility in the heads allows the detached head to diffuse forward and attach further along the filament than the working stroke has carried it. A stride of 36 nm correlates well with the average steps (~34–38 nm) measured in optical trap experiments when a succession of steps is seen[10]. This indicates that the structural basis of stepping is a succession of strides between sites on actin rather than the working strokes of the heads themselves. In molecules attached by a single head, a variety of attachment angles is apparent (Fig. 1e). After assignment of the actin polarity, some are near the rigor angle, but others are found to be tilted in the same direction as the lead head of the doubly-attached molecules, and therefore appear to be molecules caught at the start of their working stroke.

Note added in proof: The doubly attached conformation seen here is similar to a recently published atomic model of this complex extrapolated from crystal structure data of actin subunits and myosin II heads in rigor and ADP–AlF_4 states[27]. □

Received 10 February; accepted 19 April 2000.

1. Sellers, J. R. *Myosins* (Oxford Univ. Press, Oxford, 1999).
2. Rayment, I. *et al.* Three-dimensional structure of myosin subfragment-1: a molecular motor. *Science* **261,** 50–58 (1993).
3. Craig, R. *et al.* Electron microscopy of thin filaments decorated with a Ca^{2+}-regulated myosin. *J. Mol. Biol.* **140,** 35–55 (1980).
4. Cheney, R. E. *et al.* Brain myosin-V is a two-headed unconventional myosin with motor activity. *Cell* **75,** 13–23 (1993).
5. Howard, J. Molecular motors: structural adaptations to cellular functions. *Nature* **389,** 561–567 (1997).
6. De La Cruz, E. M., Wells, A. L., Rosenfeld, S. S., Ostap, E. M. & Sweeney, H. L. The kinetic mechanism of myosin V. *Proc. Natl Acad. Sci. USA* **96,** 13726–13731 (1999).
7. Wang, F. *et al.* Effect of ADP and ionic strength on the kinetic and motile properties of recombinant mouse myosin V. *J. Biol. Chem.* **275,** 4329–4335 (2000).
8. Howard, J., Hudspeth, A. J. & Vale, R. D. Movement of microtubules by single kinesin molecules. *Nature* **342,** 154–158 (1989).
9. Rice, S. *et al.* A structural change in the kinesin motor protein that drives motility. *Nature* **402,** 778–784 (1999).
10. Mehta, A. D. *et al.* Myosin-V is a processive actin-based motor. *Nature* **400,** 590–593 (1999).
11. Veigel, C. *et al.* Is one myosin V molecule sufficient for vesicular transport? *Biophys. J.* **78,** 242A (2000).
12. Trinick, J. & Offer, G. Cross-linking of actin filaments by heavy meromyosin. *J. Mol. Biol.* **133,** 549–556 (1979).
13. Walker, M., Trinick, J. & White, H. Millisecond time resolution electron cryo-microscopy of the M-ATP transient kinetic state of the acto-myosin ATPase. *Biophys J.* **68,** 87S–91S (1995).
14. Cheney, R. E. Purification and assay of myosin V. *Methods Enzymol.* **298,** 3–18 (1998).
15. Frank, J. *Three-Dimensional Electron Microscopy of Macromolecular Assemblies* (Academic, New York, 1996).
16. Burgess, S. A., Walker, M. L., White, H. D. & Trinick, J. Flexibility within myosin heads revealed by negative stain and single-particle analysis. *J. Cell Biol.* **139,** 675–681 (1997).
17. Burgess, S. A. *et al.* Real-space 3-D reconstruction of frozen-hydrated arthrin and actin filaments at 2 nm resolution. *Biophys. J.* **78,** 8A (2000).
18. Egelman, E. H. & DeRosier, D. J. Image analysis shows that variations in actin crossover spacings are random, not compensatory. *Biophys J.* **63,** 1299–1305 (1992).
19. Whittaker, M. *et al.* A 35-A movement of smooth muscle myosin on ADP release. *Nature* **378,** 748–751 (1995).
20. Moore, J. R., Krementsova, E., Trybus, K. M. & Warshaw, D. M. Myosin V exhibits a high duty cycle and large unitary displacement at zero load. *Biophys J.* **78,** 272A (2000).
21. Veigel, C. *et al.* The motor protein myosin-I produces its working stroke in two steps. *Nature* **398,** 530–533 (1999).
22. Sugimoto, Y., Tokunaga, M., Takezawa, Y., Ikebe, M. & Wakabayashi, K. Conformational changes of the myosin heads during hydrolysis of ATP as analyzed by x-ray solution scattering. *Biophys. J.* **68,** 29S–34S (1995).
23. Smith, C. A. & Rayment, I. X-ray structure of the magnesium(II). ADP. vanadate complex of the Dictyostelium discoideum myosin motor domain to 1.9 A resolution. *Biochemistry* **35,** 5404–5417 (1996).
24. Houdusse, A., Kalabokis, V. N., Himmel, D., Szent-Györgyi, A. G. & Cohen, C. Atomic structure of scallop myosin subfragment S1 complexed with MgADP: a novel conformation of the myosin head. *Cell* **97,** 459-470 (1999).
25. Walker, M., Knight, P. & Trinick, J. Negative staining of myosin molecules. *J. Mol. Biol.* **184,** 535–542 (1985).
26. Frank, J., Shimkin, B. & Dowse, H. SPIDER- a modular software system for electron image-processing. *Ultramicroscopy* **6,** 343–357 (1981).
27. Vale, R. D. & Milligan, R. A. The way things move: looking under the hood of molecular motor proteins. *Science* **288,** 88–95 (2000).

Acknowledgements

We thank C. Veigel, H. White and S. Schmitz for discussions and E. Harvey for technical assistance supported by BBSRC (to J.T. and P.J.K.) and NIH (to J.T. and H. White).

Correspondence and requests for materials should be addressed to P.J.K. (e-mail: p.j.knight@leeds.ac.uk). An animated sequence of images is available at http://www.leeds.ac.uk/bms/research/muscle/muscle.htm.

The lyase activity of the DNA repair protein β-polymerase protects from DNA-damage-induced cytotoxicity

Robert W. Sobol, Rajendra Prasad, Andrea Evenski, Audrey Baker, Xiao-Ping Yang, Julie K. Horton & Samuel H. Wilson

Laboratory of Structural Biology, National Institute of Environmental Health Sciences, PO Box 12233, Research Triangle Park, North Carolina 27709-2233, USA

Small DNA lesions such as oxidized or alkylated bases are repaired by the base excision repair (BER) pathway[1]. BER includes removal of the damaged base by a lesion-specific DNA glycosylase, strand scission by apurinic/apyrimidinic endonuclease, DNA resynthesis and ligation[2]. BER may be further subdivided into DNA β-polymerase (β-pol)-dependent single-nucleotide repair and β-pol-dependent or -independent long patch repair subpathways[3–6]. Two important enzymatic steps in mammalian single-nucleotide BER are contributed by β-pol: DNA resynthesis of the repair patch and lyase removal of 5′-deoxyribose phosphate (dRP)[2]. Fibroblasts from β-pol null mice are hypersensitive to monofunctional DNA-methylating agents, resulting in increases in chromosomal damage, apoptosis and necrotic cell death[3,7]. Here we show that only the dRP lyase activity of β-pol is required to reverse methylating agent hypersensitivity in β-pol null cells. These results indicate that removal of the dRP group is a pivotal step in BER *in vivo*. Persistence of the dRP moiety in DNA results in the hypersensitivity phenotype of β-pol null cells and may signal downstream events such as apoptosis and necrotic cell death.

Several DNA polymerases can support single-nucleotide and long patch BER DNA synthesis *in vitro*[4,5], indicating that other endogenous polymerases might functionally complement the β-pol deficiency in β-pol null cells. However, β-pol null cells are hypersensitive to the cytotoxic effects of the methylating agent methyl methanesulphonate (MMS)[3], indicating an absolute *in vivo* requirement for β-pol. Here we investigate this essential role of β-pol in resistance to methylating agents.

We constructed β-pol minigenes[3] to express Flag epitope-tagged variants of the enzyme that have wild-type activity or are deficient in polymerase activity, lyase activity or both (Fig. 1c). These minigenes were introduced into β-pol null cells and the resulting MMS hypersensitivity phenotype was analysed. Cells expressing wild-type β-pol (β-pol null/WT β-pol cells) were as resistant to MMS as wild-type cells, whereas control cells expressing the neomycin resistance gene (β-pol null/Neo cells) and untransfected cells were hypersensitive to MMS (Fig. 1a and b). The roles of the carboxy-terminal polymerase domain (relative molecular mass 31,000; M_r